Journal of Materials Chemistry B

PAPER

View Article Online
View Journal | View Issue

Cite this: J. Mater. Chem. B, 2014, 2, 3538

Controlled free radical generation against tumor cells by pH-responsive mesoporous silica nanocomposite†

Jingke Fu, Yingchun Zhu* and Yang Zhao

Received 10th March 2014
Accepted 30th March 2014

DOI: 10.1039/c4tb00387j

www.rsc.org/MaterialsB

Free radicals are toxic entities known to cause cellular damage and to mediate cell death. We herein develop a controlled free radical generation strategy for cancer therapy *via* pH-responsive release of benzoyl peroxide (BPO) in tumor cells and producing free radicals to mediate cell death. BPO as the free radical resource was encapsulated into a chitosan (Cs)-coated mesoporous silica nanocomposite (BPO@HMSNs-Cs). The mesoporous silica carrier improved the BPO solubility by preventing its crystallization and promoted its stability by inclusion. Chitosan imparted the nanocomposite pH-responsive BPO release capacity with enhanced BPO release in simulated acidic tumor media (pH 6.5) and minor release in simulated normal tissue media (pH 7.4). The enhanced free radical generation in tumor media further led to significantly higher cytotoxicity in the tumor at acidic pH 6.5 than at physiological pH 7.4. The free radical-mediated cytotoxicity of BPO@HMSNs-Cs was verified by the observation of free radical-induced green fluorescence in cells. This pH-responsive free radical generation nanocomposite may provide new opportunities for controlled drug delivery and cancer therapy.

Introduction

Free radicals are toxic entities known to cause cellular damage and to mediate cell death. Excess free radicals induce oxidative modification of cellular biomolecules, inhibit protein function, produce breakage in DNA strands and promote cells death.[1–4] Destruction of cells by irradiation-induced free radical generation has proved to be an effective intervention strategy in cancer therapy. An alternative is, in principle, drug-induced free radical generation. Some conventional anticancer drugs, such as doxorubicin,[5] 2-methoxyestradiol,[6] arsenic trioxide[7] and bleomycin,[8] were shown to partially exert their cytotoxicity by induction of free radical generation. Thus, continuous free radical generation in the vicinity of tumor cells could be potentially employed as a desirable therapeutic principle.

Benzoyl peroxide (BPO) is a widely used free radical generating compound found principally in plastic and rubber industries as a free radical initiator, which rapidly generates free radical species under thermal or irradiation stimulation. Because of its free radical generating property,[9] BPO can be utilized as a free radical resource for free radical generation strategy in cancer intervention. Nevertheless, BPO is sensitive to heat/irradiation and is chemically unstable in numerous solvents. Decomposition of BPO to form benzoic acid (BA) and other side products has been demonstrated to proceed *via* a rapid free radical mechanism arising from the instability of the O–O bond (bond energy: 120 kJ mol^{-1}) in the BPO molecule.[10] This decomposition makes the therapeutic employment of BPO difficult since it may drastically degrade to reactive free radicals before it reaches its desired targets. In addition, BPO is poorly soluble in aqueous media (water solubility: 9.1 mg L^{-1} at 25 °C),[11] which further restricts its oral or subcutaneous applications. Therefore, a regimen to improve the chemical stability of BPO with increased aqueous solubility and controlled delivery properties is desirable; however, it has not yet been reported.

The formulation of BPO in a carrier is an attractive protocol with many potential advantages, including enhanced chemical stability, improved aqueous solubility, controlled delivery and tumor targeting. Numerous types of carriers, such as liposomes,[12] microspheres[13] and polymers,[14] have been adopted to store and deliver BPO. However, low BPO encapsulation efficiency, as well as the poor chemical stability of these organic carriers, has restricted their clinical applications. Alternatively, inorganic mesoporous silica nanocarriers have attracted widespread attention in catalysis,[15] bio-imaging[16–18] and drug/gene delivery[19–23] due to their high chemical and thermal stability, excellent biocompatibility and favorable degradability.[24–27] Among them, hollow mesoporous silica nanoparticles (HMSNs) are of particular interest due to their large surface area/pore volume and huge hollow cavities with high guest-loading capacities. Furthermore, the surfaces of HMSNs could be

Key Lab of Inorganic Coating Materials, Shanghai Institute of Ceramics, Chinese Academy of Sciences, 1295 Dingxi Road, Shanghai 200050, China. E-mail: yzhu@mail.sic.ac.cn

† Electronic supplementary information (ESI) available: Figures and characterization of as-prepared compounds. See DOI: 10.1039/c4tb00387j

tethered with various functional motifs, endowing HMSNs with a stimuli-responsive cargo-release property.[28–32] All these above features together with the increased passive delivery of these nanoparticles into tumor cells by the enhanced permeation and retention (EPR) effect[33] make HMSNs an ideal carrier for this labile peroxide.

In this report, we develop a controlled free radical generation strategy for cancer therapy *via* pH-responsive release of BPO as the free radical resource, which selectively generates free radicals in acidic tumor media and exerts enhanced toxicological effect against tumor cells. HMSNs with large hollow cavities and abundant mesoporous channels were utilized as carriers to load a poorly soluble BPO (BPO@HMSNs), which could be effectively transported into tumor cells and improve the therapeutic efficiency of BPO in a human breast carcinoma cell line (ZR75-30). Moreover, the mesoporous silica carrier was shown to improve the solubility and stability of BPO by preventing its crystallization and stabilizing the amorphous BPO therein. In order to selectively release BPO, the surface of BPO@HMSNs was wrapped with pH-responsive chitosan (Cs) layers (BPO@HMSNs-Cs). Enhanced BPO release was realized in simulated acidic tumor media (pH 6.5) and subcellular endosomes (pH 5.0), whereas minor release occurred in simulated normal tissues (pH 7.4). This pH-dependent BPO release further led to significantly higher BPO@HMSNs-Cs cytotoxicity in the tumor at acidic pH 6.5 than that at physiological pH 7.4. The free radical-mediated toxicological effect of BPO@HMSNs-Cs was demonstrated by the observation of strong green luminescence in cells, which was induced by the reaction of oxygen free radicals with DCFH-DA. To the best of our knowledge, this is the first report on controlled free radical generation for cancer therapy *via* selective generation of toxic free radicals in acidic tumor media. This pH-responsive hybrid nanocomposite may provide new opportunities for controlled drug delivery and cancer therapy.

Experimental section

Materials

Cetyltrimethyl ammonium bromide (C_{16}TAB), tetraethyl orthosilicate (TEOS), ammonium hydroxide (NH_4OH, 25–28%), sodium carbonate (Na_2CO_3) and chitosan (Cs, deacetylation degree >92%, BR) were obtained from Sinopharm Chemical Reagent Co., Ltd. Gamma-glycidoxypropyltrimethoxysilane (γ-GPTMS), benzoyl peroxide (BPO, 75%, remainder water) and benzoic acid (BA) were purchased from Sigma-Aldrich. Phosphate buffer solution (PBS), penicillin–streptomycin solution and RPMI-1640 medium were purchased from Gibco. 3-(4,5-Dimethylthiazol-2-yl)-2,5-diphenyltetrazolium bromide (MTT) and 2′,7′-dichlorodihydrofluorescein diacetate (DCFH-DA) were obtained from Sigma. For the experiments, a stock solution of DCFH-DA (10 mM, in DMSO) was prepared and kept at −20 °C in the dark for further use. Fetal bovine serum (FBS) was purchased from Sijiqing Biotechnology Ltd. All reagents were used as received without further purification. Deionized water was used in all experiments, whereas ultrapure water filtrated by a 0.22 μm filter was used in cell experiments.

Synthesis of hollow mesoporous silica nanoparticles (HMSNs)

A typical synthesis of hollow mesoporous silica nanoparticles (HMSNs) involves two steps, as described in previous studies.[34,35] Firstly, solid silica nanoparticles (SSNs) were prepared as the hard template for further etching. EtOH (74 mL), H_2O (10 mL) and ammonium hydroxide (3.14 mL) were mixed at 30 °C. Then, TEOS (6 mL) was quickly added, and the mixture was stirred for 1 h. The obtained SSNs were collected by centrifugation, washed with EtOH, and dried under vacuum. Next, the as-prepared SSNs (200 mg) were dispersed into deionized water (40 mL) and sonicated for 15 min. C_{16}TAB (300 mg), H_2O (60 mL), EtOH (60 mL) and ammonium hydroxide (1.3 mL) were mixed at ambient temperature. Then, the mixture was added into the SSN suspension and was sonicated for another 1 h. TEOS (0.53 mL) was quickly injected into the above suspension, and the mixture was stirred for 7 h. The product was centrifuged and then re-dispersed into a Na_2CO_3 aqueous solution (0.4 M) and etched for 13 h at 50 °C. The resulting precipitates were collected by centrifugation, washed with excess EtOH, and dried under vacuum.

The templates C_{16}TAB in the mesoporous channels were removed by an ion-exchange procedure. Typically, the obtained nanospheres (0.5 g) were suspended into a solution containing 95% EtOH (75 mL) with NH_4NO_3 (0.2 g) with magnetic stirring and incubated for 5 h at 60 °C. The solid was then separated by centrifugation, extensively washed with EtOH, and dried under vacuum. This procedure was repeated to completely remove the templates. The template-free products were designated as HMSNs.

Preparation of BPO@HMSNs-Cs

The preparation of BPO-loaded and Cs-coated HMSNs (BPO@HMSNs-Cs) is based on an acid-catalyzed amino-oxirane addition reaction between Cs and γ-GPTMS modified HMSNs (HMSNs-G). The typical procedures were modified on the basis of previously reported methods.[36,37] Firstly, dried HMSNs (0.20 g) were dispersed in toluene (10 mL) and sonicated for 15 min. Then, γ-GPTMS (5 mL) was added into the mixture and refluxed for 5 h in dry nitrogen. At the end of the reaction, the obtained HMSNs-G was collected by centrifugation, washed with acetone, and dried under vacuum for further use. Secondly, BPO was loaded into HMSNs-G by dispersing the as-prepared HMSNs-G (0.1 g) into a BPO/EtOH solution (15.0 mg mL^{-1}) in a flask. The mixture was sealed and stirred for 12 h at ambient temperature in the dark. BPO-loaded HMSNs-G (BPO@HMSNs-G) was then separated by centrifugation, washed with water, and freeze-dried in the dark. Finally, the obtained BPO@HMSNs-G was coated with Cs polyelectrolytes to avoid the pre-release of BPO. Briefly, Cs was dissolved into an acetic acid aqueous solution (10% v/v, 10 mL) and stirred for 48 h at room temperature, followed by pH adjustment to 5.0 with 2 M NaOH. Afterwards, BPO@HMSNs-G (0.1 g) was added to the Cs colloids and was stirred in the dark for 12 h. Then, the mixture was adjusted to pH 7.4 by 1 M NaOH and was stirred for another 2 h. Cs molecules were deprotonated and changed from a flexibly entangled state to an orderly aggregated state, which efficiently

restricted the release of BPO from the carrier. Finally, BPO@HMSNs-Cs were obtained by centrifugation, washed with PBS (pH 7.4), and dried under vacuum.

For comparison, the encapsulation of BPO in naked HMSNs (BPO@HMSNs) and the coating of Cs on naked HMSNs (HMSNs-Cs) were performed with a similar procedure.

Evaluation of BPO loading capacity and BPO stability of the fabricated nanocomposites

The amount of BPO incorporated in BPO@HMSNs was determined by monitoring the UV/vis absorbance before and after the encapsulation of BPO in EtOH. A BPO calibration curve was prepared in an EtOH solution ($\lambda_{max} = 234$ nm, $r = 0.9989$). The BPO loading capacity in BPO@HMSNs-Cs was quantified with a similar procedure. To be specific, after collecting the obtained BPO@HMSNs-Cs by centrifugation, the supernatant was withdrawn. Then, EtOH (10.0 mL) was added to dissolve the BPO in the supernatant. After filtration over a 0.45 μm membrane filter, the filtrate was measured by a UV/vis spectrophotometer at 234 nm to evaluate the BPO leak during the Cs-coating process. The BPO-loading capacity of BPO@HMSNs-Cs was calculated by subtracting the leakage from BPO@HMSNs during the Cs-coating process.

In order to examine the integrity of BPO after Cs coating, the as-prepared BPO@HMSNs-Cs was monitored by a UV/vis spectrophotometer. Typically, BPO@HMSNs-Cs (2 mg) was dispersed into EtOH (2 mL), and the suspension was stirred in the dark for 2 h to release the loaded BPO. Then, the suspension was filtered through a 0.45 μm membrane filter, and the components were determined by UV/vis analysis.

For comparison, free BPO and benzoic acid (BA, the major stable metabolite of BPO) were also dissolved in EtOH and were monitored by a UV/vis spectrophotometer with a similar procedure.

pH-responsive BPO release profiles in different buffer solutions (pH 7.4, 6.5, 5.0)

The BPO release was monitored by UV/vis spectrophotometer, and the cargo-release procedure was performed as follows: the as-prepared dehydrated BPO@HMSNs and BPO@HMSNs-Cs were both divided into three moieties with accurate weight, and then suspended in centrifuge tubes with different PBS (pH 7.4, 6.5, 5.0) under sink conditions, which was accomplished by adding 0.08% (w/v) sodium lauryl sulfate (SLS) to the PBS release media. The tubes were maintained at ambient temperature and left incubated on a shaking table (shaking speed: 100 rpm) in the dark. After a given time interval, the tubes were centrifuged at 5000 rpm for 5 min. The supernatant (3.0 mL) was extracted from each test tube and was replaced by a fresh release medium (3.0 mL). The extracted medium was diluted for UV/vis analysis at a predetermined time course. All analyses were performed in triplicate. Each dataset represented the average of three measurements, and the error was expressed as standard deviation (SD).

To compare the cargo-release profile of BPO-loaded HMSNs nanocomposite with that of its corresponding crystalline material, the dissolution profile of crystalline BPO was also detected under the same conditions.

Furthermore, to examine the integrity of BPO during and after the release process, the release media (10.0 μL) were extracted at the end of the BPO release and diluted with isopropanol (10.0 mL). The mixture was then filtered and analyzed by HPLC with an AB-H column (Daicel Chemical Industries, Ltd. Japan). Isopropanol–hexane (1 : 9, v/v) was used as the eluent. The column effluent was monitored at 221 nm with a UV detector. Free BPO and BA were also monitored by HPLC as the contrast samples under the same conditions.

Cell culture

Human breast carcinoma cell line ZR75-30 was purchased from the cell bank of the Chinese Academy of Sciences. Cells were cultured in an RPMI-1640 medium (pH 7.4), supplemented with 10% heat-inactivated fetal bovine serum (FBS) and maintained in a humid atmosphere with 5.0% CO_2 at 37 °C.

In vitro cytotoxicity assay

MTT reduction assay was performed to evaluate the *in vitro* cytotoxicity of free BPO, BPO@HMSNs and BPO@HMSNs-Cs against cancer cells. ZR75-30 cells were seeded in 96-well plates at a density of 5.0×10^4 cells per mL and were cultured in the RPMI-1640 medium supplemented with 10% FBS at 37 °C in a humid 5% CO_2 atmosphere. After 24 h incubation, the culture media were replaced with exposure media consisting of fresh culture media supplemented with 10% FBS, 1% penicillin–streptomycin solution, and sample of free BPO or BPO-loaded nanocomposite (BPO@HMSNs or BPO@HMSNs-Cs) with equivalent BPO concentrations (4, 8 and 16 μg mL^{-1}). After another 24 h co-incubation, the exposure media were discarded and washed twice with cold PBS (pH 7.4). Then, 20 μL of MTT (5 mg mL^{-1} in PBS) was added to each well, and the cells were further incubated for 4 h at 37 °C. Afterwards, the media were replaced with dimethyl sulfoxide (DMSO, 150 μL per well) and were gently shaken for 5 min. The absorbance was monitored by a microplate reader (Bio-Tek ELx800) at a wavelength of 490 nm. Similar culture media without samples were used as negative controls. The cytotoxicity was quantified as the percentage of cell viability relative to the negative control group. Each data point was represented as means ± SD of six independent experiments.

Taking into account the pH-relevant BPO release profiles of the BPO-loaded nanocomposites, the cell toxicity of these nanocomposites were expected to be pH-dependent. For this purpose, the RPMI-1640 medium (pH 6.5) adjusted by 1 M HCl was chosen to simulate the acid tumor microenvironment, and the pH-dependent cell toxicity was monitored with a similar procedure.

For comparison, the *in vitro* cytotoxicity of BPO-free HMSNs and HMSNs-Cs were evaluated with a similar protocol. HMSNs and HMSNs-Cs were suspended into a fresh RPMI-1640 culture medium with HMSN and HMSNs-Cs concentrations of 25, 50, 100 and 200 μg mL^{-1}.

To further identify the pharmacological activity of BPO released from the cargo-loaded nanocomposites. Benzoic acid

(BA), the major stable metabolite of BPO,[38] was also investigated by MTT assay with BA concentrations of 8, 16, 32 and 64 μg mL^{-1}.

In vitro detection of free radical production using DCFH-DA

Free radicals were measured by using a non-fluorescent probe, 2′,7′-dichlorodihydrofluorescein diacetate (DCFH-DA), which penetrates into cells where it is cleaved and oxidized by oxygen free radicals to highly fluorescent 2′,7′-dichlorofluorescein (DCF).[39] The DCF fluorescence was then recorded by inverted fluorescence microscopy. Briefly, ZR75-30 cells were exposed to serum-free media with BPO@HMSNs-Cs (140 μg mL^{-1}, containing 16 μg mL^{-1} of BPO), HMSNs-Cs (100 μg mL^{-1}) or BA (16 μg mL^{-1}). After 4 h incubation at 37 °C, the culture media were discarded, and DCFH-DA (20 μM, 10 μL per well) was added. Then, cells were incubated for another 30 min. After being washed carefully with PBS (pH 7.4) twice, the fluorescence was observed by fluorescence microscopy.

Microscopic observation of ZR75-30 cells morphology

Cell morphology was observed by inverted microscopy to make comparative analyses in cell morphology before and after the sample treatment. Briefly, ZR75-30 cells were cultured in the RPMI-1640 medium supplemented with 10% FBS at 37 °C in a humid 5% CO_2 atmosphere. After 24 h, cell morphology was recorded by inverted microscopy. Then, the cells were exposed to culture media containing BPO@HMSNs-Cs (140 μg mL^{-1}, containing 16 μg mL^{-1} of BPO) or free BA (64 μg mL^{-1}). Cell morphology was then observed by microscope after 24 h incubation.

Characterization

The morphology, size and element analysis of the samples (HMSNs and HMSNs-Cs) were obtained by transmission electron microscope (TEM, JEM-2100F, Japan) equipped with an X-ray energy dispersive spectrometer (EDS). A powder X-ray diffraction (XRD) pattern was recorded on a diffractometer (Rigaku Ultima IV, Japan) with Cu Kα radiation. N_2 adsorption–desorption isotherm measurement was carried out on a Micrometitics Tristar 3000 nitrogen adsorption apparatus. Surface area and pore volume were determined by BET analysis. Zeta potential was determined using the Zetasizer Nano Series (Malvern, Zetasizer-3000HS). Fourier transform infrared (FTIR, Shimadzu, Japan) analysis was performed using KBr discs in the region of 4000–400 cm^{-1}. The UV/vis absorption spectrum was recorded on a UV-3101 Spectrophotometer (Shimadzu, Japan). Thermogravimetry (TG) and differential scanning calorimetry (DSC) were carried out on a TA thermal analyzer at a heating rate of 5 °C min^{-1} in air. Cell morphology and free radical production were analyzed using an inverted fluorescence microscope (Olympus IX71, Japan).

Statistical analysis

Data were presented as means ± SDs from at least six independent experiments. Statistical analyses were performed using SPSS software (version 19.0). Statistical comparisons were performed using Student's *t*-test. $P < 0.05$ was used to establish statistical significance.

Results and discussion

Preparation and characterization of BPO@HMSNs-Cs

The preparation of BPO@HMSNs-Cs involved four steps. Firstly, mono-dispersed HMSNs were fabricated based on selective etching strategy. Then, γ-GPTMS was conjugated onto HMSNs (HMSNs-G) for further reaction with chitosan. Afterwards, BPO was encapsulated into HMSNs-G (BPO@HMSNs-G) by simple molecule diffusion in EtOH. Finally, chitosan (Cs) was coated onto BPO@HMSNs-G (BPO@HMSNs-Cs) for pH-responsive release of guests. The whole procedure is illustrated in Scheme 1.

The morphology of HMSNs before and after the coating of Cs was examined by TEM. As shown in Fig. 1a, the as-prepared HMSNs were well-dispersed spheres with an average diameter around 350 nm. The magnified TEM image in Fig. 1c indicates that the spheres are hollow with an oriented mesoporous shell of about 80 nm. In order to realize controlled release of cargos, pH-responsive Cs polyelectrolyte was introduced onto the HMSNs. The observed polymer layers on the surfaces of the HMSNs (Fig. 1b and d) illustrate the successful coating of Cs around the HMSNs. The EDS element analysis in Fig. 1e shows that the as-prepared HMSNs are simply composed of Si and O. However, an obvious C signal was found in HMSNs-Cs (Fig. 1f), which could be attributed to the γ-GPTMS and/or Cs layers on the surface of HMSNs-Cs.

The chemical structures of HMSNs, BPO@HMSNs and BPO@HMSNs-Cs were examined with FTIR. For the sake of simplification, the low energy range (2000–400 cm^{-1}), which is richer in information, is discussed. As shown in Fig. 2a, the as-prepared HMSNs showed characteristic bands of silica at 1228, 1080, 968 and 797 cm^{-1}, which can be attributed to the asymmetric stretching vibrations of Si–O–Si at 1228 and 1080 cm^{-1}, the symmetric stretching vibration of Si–O–Si at 794 cm^{-1} and the stretching vibration of Si–OH at 968 cm^{-1}.[40,41] Fig. 2e shows the IR spectrum of native BPO, which exhibited a series of peaks at 1760, 1228, 1000 and 706 cm^{-1}. Based on their positions, the observed bands can be assigned to the carbonyl group ($\nu_{C=O}$ at 1760 cm^{-1}), the aromatic ring ($\nu_{C=C}$ at 1600–1450 cm^{-1} and δ_{C-H} at 706 cm^{-1}) and the benzoyl group vibrations (ν_{C-O} at 1228 and 1000 cm^{-1}).[42] The IR spectra of BPO@HMSNs (Fig. 2b) and BPO@HMSNs-Cs (Fig. 2c) were almost coincident with that of native BPO (Fig. 2e), confirming the presence and the structural integrity of BPO in these nanocomposites. Furthermore, new peaks of native Cs (Fig. 2d) at about 1650, 1380 and 1089 cm^{-1}, which are attributed to the amide ($\nu_{C=O}$), δ_{CH3} and ν_{C-O} vibrations,[40,43] appeared in BPO@HMSNs-Cs, indicating the successful modification of Cs in BPO@HMSNs-Cs.

The N_2 adsorption–desorption isotherm technique was adopted to reveal the effects of Cs coating and BPO storage on the porosity of HMSNs. As shown in Fig. S1,† the as-prepared HMSNs exhibited a typical Langmuir type IV isotherm with a sharp capillary condensation relative pressure (P/P_0) between 0.3 and 0.4, which is characteristic of a well-defined mesoporous structure. The N_2 adsorption–desorption isotherm after

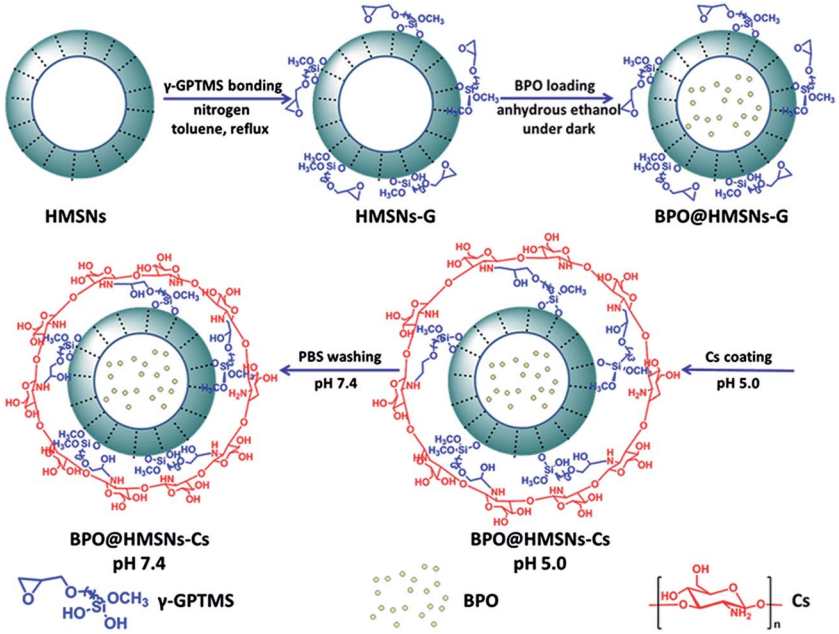

Scheme 1 Illustration of the fabrication of BPO@HMSNs-Cs nanocomposite. Firstly, γ-GPTMS was decorated onto the as-prepared HMSNs (HMSNs-G). Then, BPO was encapsulated into HMSNs-G *via* simple molecule diffusion in a BPO/EtOH solution (BPO@HMSNs-G). Finally, Cs polyelectrolyte was modified onto BPO@HMSNs-G based on an acid-catalyzed amino-oxirane addition reaction between Cs and γ-GPTMS at pH 5.0. Upon exposure to a neutral medium (pH 7.4), Cs polyelectrolyte was deprotonated and collapsed to an orderly aggregated state, which blocks and encapsulates BPO inside the nanocarrier (BPO@HMSNs-Cs).

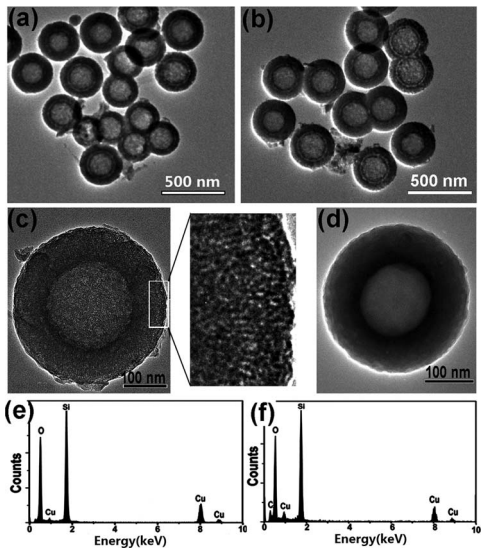

Fig. 1 TEM images of (a and c) HMSNs and (b and d) HMSNs-Cs. EDS spectra of (e) HMSNs and (f) HMSNs-Cs.

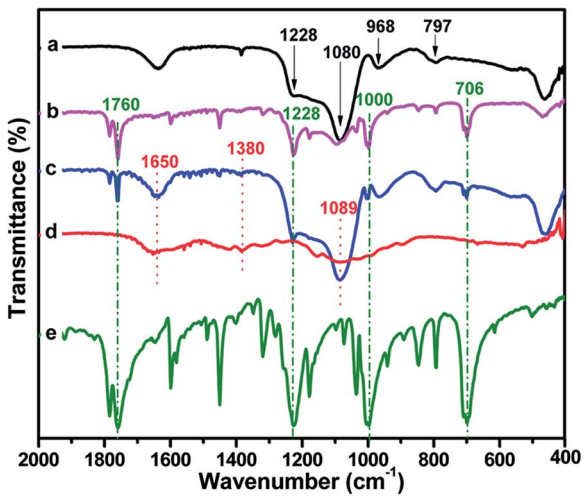

Fig. 2 FTIR spectra of (a) HMSNs, (b) HMSNs after BPO loading (BPO@HMSNs), (c) HMSNs after BPO loading and Cs coating (BPO@HMSNs-Cs), (d) Cs and (e) BPO.

the γ-GPTMS modification (HMSNs-G) was almost consistent with the HMSNs matrix, indicating the well-defined mesoporous structure in HMSNs-G. By contrast, lowered P/P_0 was observed in BPO@HMSNs, and almost no relative pressure leap was detected in BPO@HMSNs-Cs. BET measurement showed that the surface area (S_{BET}) and pore volume (V_{pore}) of HMSNs was 1026 $m^2\ g^{-1}$ and 0.79 $cm^3\ g^{-1}$, respectively, which was reduced to 243 $m^2\ g^{-1}$ and 0.19 $cm^3\ g^{-1}$ after BPO-loading, with a further reduction to 87 $m^2\ g^{-1}$ and 0.12 $cm^3\ g^{-1}$ after Cs coating (Table 1). It can be inferred that some BPO molecules were stored in the mesoporous channels and that Cs layers were coated on the pore outlets of HMSNs in BPO@HMSNs-Cs. The pore-size distribution curves (Fig. S1†) showed that the pore diameters of HMSNs were centered at 2.8 nm and remained constant at 2.6 nm in HMSNs-G. However, a distinct pore-size reduction to 2.0 nm was apparent after BPO loading and almost no pores could be detected after Cs coating. All of these results

Table 1 Structure parameters, BPO-loading efficiency and zeta potential analyses of the fabricated samples (HMSNs, HMSNs-G, BPO@HMSNs and BPO@HMSNs-Cs)

Sample	S_{BET} [m^2 g^{-1}]	V_{Pore} [cm^3 g^{-1}]	D_{Pore} [nm]	BPO-loading efficiency	Zeta potential[c] [mV]
HMSNs	1026	0.79	2.8	—	−38.2 ± 2.1
HMSNs-G	1058	0.77	2.6	—	—
BPO@H[a]	243	0.19	2.0	14.6%	−46.0 ± 1.6
BPO@H-Cs[b]	87	0.12	—	11.2%	+6.3 ± 2.7

[a] Abbreviation for BPO@HMSNs. [b] Abbreviation for BPO@HMSNs-Cs. [c] Zeta potentials were measured in PBS (pH 7.4) at room temperature. Data were presented as means ± SDs (n = 3).

indicated the successful loading of BPO and coating of Cs in BPO@HMSNs-Cs. The specific structure parameters of HMSNs, HMSNs-G, BPO@HMSNs and BPO@HMSNs-Cs determined by the Barrett–Joyner–Halenda (BJH) method are presented in Table 1.

Zeta potential analysis was utilized to determine the potential difference before and after cargo loading and polyelectrolyte coating. As shown in Table 1, HMSNs exhibited a negative potential of about −38.2 mV at pH 7.4. It has been reported that nanoparticles with zeta potentials above (±) 30 mV are stable in suspensions, which indicates that the as-prepared HMSNs exhibited stable aqueous dispersion in a physiological environment (pH 7.4). After further BPO loading and Cs coating, the zeta potential of BPO@HMSNs-Cs increased to +6.3 mV due to the presence of the cationic Cs polyelectrolyte. Considering the fact that cancer cell surfaces are negatively charged,[44] cationic BPO@HMSNs-Cs would more easily bind to cancer cell membranes, which further leads to more efficient cargo delivery.

Evaluation of BPO-loading capacity and BPO stability

BPO was loaded into HMSNs by simple molecular diffusion in a BPO/EtOH solution. The loading capacity of BPO@HMSNs was determined by UV/vis spectrophotometer. BPO exhibited an obvious absorption peak at 234 nm in EtOH (Fig. S2†). The BPO in BPO@HMSNs was quantified by monitoring the relative absorbance data at 234 nm. The calculated BPO loading capacity of BPO@HMSNs was 14.6%, as listed in Table 1. After immersing the obtained BPO@HMSNs into 10% Cs colloids for 24 h, the BPO leakage during the Cs-coating process was determined by UV/vis spectrophotometer. The loading capacity of BPO@HMSNs-Cs was 11.2%, which was calculated by subtracting the BPO leakage from BPO@HMSNs during the Cs-coating process.

The BPO integrity in the as-prepared BPO@HMSNs-Cs was examined by UV/vis spectrophotometer. As shown in Fig. S2,† the obtained BPO@HMSNs-Cs exhibited an absorption peak at 234 nm in EtOH, which is consistent with the intact BPO in EtOH. Fig. S2† shows that benzoic acid (the major stable metabolite of BPO) presented an obvious absorption peak at 227 nm in EtOH. These results collectively confirm that the BPO was intact and did not react with Cs during the preparation of BPO@HMSNs-Cs.

Enhancement of BPO dissolution in aqueous solution by loading of BPO into HMSNs

BPO is characterized by poor aqueous solubility, which affects its pharmacological activity and bioavailability. The poor dissolution rate of the BPO is associated with its highly ordered crystalline structure whose disruption requires high energy. An emerging effective approach to enhance the dissolution of a poorly soluble drug is the prevention of drug crystallization by its inclusion in ordered mesoporous silica. Previous studies demonstrated the applicability of ordered mesoporous silica as an excipient in the release enhancement of a series of poorly soluble compounds.[45,46] Fig. 3 shows the BPO release from the as-prepared BPO@HMSNs in PBS (pH 7.4) under sink conditions, which was compared with that of its corresponding crystalline counterpart (crystalline BPO). It can be seen that after 165 min, the BPO release from BPO@HMSNs reached 84.1% in pH 7.4 PBS, while from the crystalline counterpart the BPO release was only 35.4%. It is clear that the nanocomposite showed remarkable improvement in BPO dissolution rates in an aqueous medium. It is reported that the amorphous form of a drug often shows improved solubility, compared with its crystalline counterpart, and the conversion of crystalline form into an amorphous state was proposed to improve drug dissolution. It was speculated the amorphous BPO in the ordered mesoporous silica led to the observed BPO dissolution improvement. As a proof of this concept, powder XRD analysis was performed to evaluate the presence or absence of BPO crystals in the composite. As shown in Fig. S3,† the as-prepared BPO@HMSNs showed only typical reflection of HMSNs and no peaks attributable to crystalline BPO. However, the BPO–HMSNs physical mixture (with BPO proportional to the BPO in BPO@HMSNs) showed a distinct reflection of crystalline BPO. These results verified that the loading procedure inhibited the

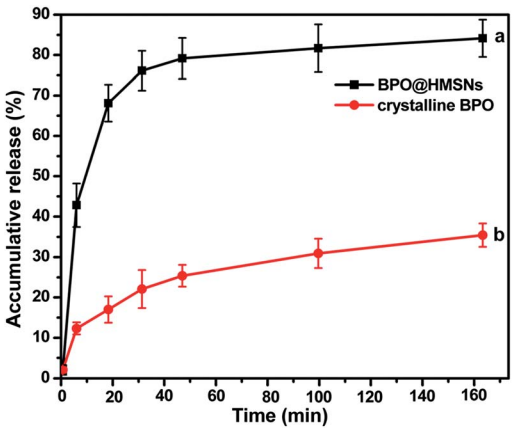

Fig. 3 Release profile of BPO from (a) BPO@HMSNs and (b) crystalline BPO in PBS (pH 7.4) under sink conditions. The results depicted were represented as means ± SDs (n = 3). BPO in the nanocomposite (BPO@HMSNs) exhibited a clear enhancement of dissolution compared with its crystalline counterpart.

crystallization of the entrapped BPO molecules in the HMSNs. The lack of crystalline BPO in BPO@HMSNs was further confirmed by differential scanning calorimetry (DSC). Fig. S4† compared the DSC results of the as-prepared nanocomposite with the crystalline BPO. The melting of crystalline BPO was clearly visible at 103 °C, whereas the BPO@HMSNs showed no peaks relative to BPO melting, further proving that crystallization of the confined BPO in BPO@HMSNs had not occurred.

Evaluation of pH-responsive BPO release profiles in different buffer solutions (pH 7.4, 6.5, 5.0)

The pharmacological activity of the BPO-loaded nanocomposites (BPO@HMSNs and BPO@HMSNs-Cs) was evaluated by the BPO release assay in an aqueous solution. Fig. 4 presents the BPO release profiles from BPO@HMSNs and BPO@HMSNs-Cs in different PBS (pH 7.4, 6.5, 5.0) under sink conditions. Such PBS was chosen to mimic the environment of normal tissues/blood (pH 7.4),[47] diseased tissues like inflammatory tissues/tumor cells (pH 6.5) or subcellular endosomes (pH 5.0). As shown in Fig. 4, the release of BPO from both nanocomposites exhibited a typical sustained manner, whereas the release rate was distinctly different. Fig. 4a is the BPO release curves from BPO@HMSNs in different PBS. It is clearly observed that the BPO release was unconfined and analogous in different PBS. The cumulative release amount was about 84.1% at pH 7.4, 83.8% at pH 6.5 and 81.4% at pH 5.0 after 165 min. As can be seen from the crystal data[48] listed in the inset of Fig. 4a, the size of the BPO molecule was much smaller than the pore size of HMSNs (*ca.* 2.8 nm). The uncoated pores of HMSNs thus had no confinement of BPO from the mesoporous channels. By contrast, after the coating of the Cs layers, the BPO release from BPO@HMSNs-Cs was distinctly different and had changed dramatically with the pH of the release media. BPO released from BPO@HMSNs-Cs was about 60.4% at pH 7.4, 65.9% at pH 6.5 and 80.6% at pH 5.0 after 165 min (Fig. 4b). This restrained and pH-relevant release could be attributed to the distinct flexibility and swelling behavior of Cs in different pH environments. The ionization degree of amino groups on Cs (pK_a 6.3)[49] exhibits high pH dependence. When the pH value of the release media was adjusted to 7.4, Cs chains were in an orderly aggregated state.[50] At this state, Cs molecules crystallize in an orthorhombic unit cell with the dimensions $a = 8.95(4)$, $b = 16.97(6)$, c (fiber axis) $= 10.34(4)$ Å (inset of Fig. 4a),[50,51] which could efficiently block the pores of HMSNs and hinder the release of BPO.

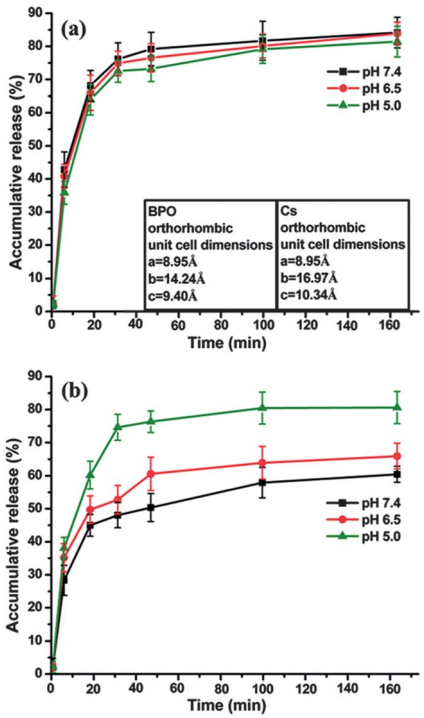

Fig. 4 BPO release profiles from (a) BPO@HMSNs and (b) BPO@HSMNs-Cs in different PBS. BPO@HMSNs presented a sustained and unconfined release profile. The BPO cumulative release amount was 84.1%, 83.8% and 81.4% at pH 7.4, 6.5 and 5.0, respectively, after 165 min, which was of little relevance to the pH of the release media. After the coating of Cs layers, pH-responsive BPO release profile was achieved with fast release in simulated diseased tissues (pH 6.5) and intracellular environment (pH 5.0), whereas minor release was achieved in simulated normal tissues (pH 7.4). BPO cumulative release amount from BPO@HMSNs-Cs was 60.4% at pH 7.4, 65.9% at pH 6.5 and 80.6% at pH 5.0 after 165 min.

Upon exposure to acidic microenvironments (pH 6.5), the amino groups in Cs were partially protonated. To compensate for excess charge, counterions were assembled on the surface of Cs polyelectrolyte. The resulting increased osmotic pressure promoted more water molecules to permeate into the polyelectrolyte from the bulk solution.[51,52] Subsequently, Cs layers swelled to a loose porous structure and transformed from an orderly aggregated state to a heavily entangled state,[36] which would partially liberate the pore outlets and lead to the fast release. When the pH value of the release media was further reduced to 5.0, Cs exhibited a more positive charge and the polymer chains presented a slightly flexible state. The destroyed regular packing between Cs chains opened the pores of HMSNs and led to the faster release of the BPO. The cumulative release amount at pH 5.0 was approximately 80.6%, which was about 1.3 times of that at pH 7.4. Based on the results above, it can be concluded that Cs imparted the HMSNs matrix with a pH-responsive-controlled release feature; *i.e.*, fast release was realized in simulated diseased tissues and subcellular endosomes, whereas minor release was seen in a simulated, normal tissue microenvironment. This pH-responsive-controlled release strategy could increase the therapeutic efficacy of BPO and mitigate its side effects to normal tissues.

Evaluation of BPO stability in BPO-loaded nanocomposites

Taking into account that BPO is sensitive to heat/irradiation and chemically unstable in numerous solvents, it is essential to evaluate the physicochemical stability of the as-prepared BPO-loaded nanocomposites. The BPO stability in the as-prepared BPO@HMSNs-Cs was examined (see above), which demonstrated that the BPO in BPO@HMSNs-Cs remained intact and did not react with Cs during the preparation process. Furthermore, in order to explore the integrity of BPO after the release assay, the final release medium was analyzed by HPLC. As shown in Fig. S5,† the HPLC of the final release medium was

consistent with that of the intact BPO, and no extra peaks in the chromatogram were detected, which demonstrated the preservation of the chemical stability of BPO during and after the release process. Previous studies have shown that mesoporous silica materials loaded with drugs could stabilize the disordered form of the drugs.[45,46] The amorphous BPO trapped in the nanoscale mesopores of silica was stabilized therein. Moreover, it has been reported that the silanol groups on the surface of the silica interacted with the benzoyl carbonyl groups of BPO.[46] The interaction between the BPO molecules and the surfaces of the carriers may contribute to the stabilization of the amorphous BPO in the composites.

MTT assay

The *in vitro* cytotoxicity of free BPO, BPO@HMSNs and BPO@HMSNs-Cs against ZR75-30 cells was investigated by the MTT assay to examine the pharmacological activity of free BPO and BPO released from the cargo-loaded nanocomposites. As shown in Fig. 5a, the cytotoxic effects of both free BPO and BPO-loaded nanocomposites increased with increasing concentrations of the samples. Notably, BPO-loaded nanocomposites exhibited higher cytotoxic effects against cancer cells compared with free BPO with equivalent BPO concentration (4, 8 or 16 μg mL^{-1}). The 24 h cell viability was 94.6% with free BPO, and it was 70.0% and 73.8% with BPO-loaded nanocomposites (BPO@HMSNs and BPO@HMSNs-Cs), respectively, at 4 μg mL^{-1} of BPO. Similar results were obtained at BPO concentrations of 8 and 16 μg mL^{-1}, as shown in Fig. 5b. The observed cytotoxicity difference between free BPO and BPO-loaded nanocomposites may be partly attributed to the distinct cell uptake mechanism. Free BPO molecules are internalized into cells generally *via* a passive diffusion-dependent process.[53] The poor solubility of BPO limits its internalization into the cellular microenvironment. By contrast, the uptake of silica nanoparticles occurs through a nonspecific adsorptive endocytosis or fluid phase pinocytosis.[54,55] Moreover, silica nanoparticles have been reported to have great affinity for the head-groups of phospholipids on cell membranes,[56] which would lead to more effective nanocomposite cell uptake and higher cytotoxicity than free BPO.

For comparison, the cytotoxicity of the nanocarriers (HMSNs and HMSNs-Cs) were also evaluated by MTT assay. Both HMSNs and HMSNs-Cs showed no obvious cytotoxicity against ZR75-30 cells, even at a concentration as high as 200 μg mL^{-1} after 24 h and 48 h of incubation (Fig. S6†). These results indicated that the prepared HMSNs and HMSNs-Cs showed high biocompatibility and low toxicity to ZR75-30 cells, which was consistent with the previously reported results.[57,58]

Furthermore, the pH-responsive BPO release profile of BPO@HMSNs-Cs (Fig. 4b) was supposed to lead to pH-dependent cell toxicity. To further demonstrate the pH sensitivity of this nanocomposite, ZR75-30 cells were exposed to BPO@HMSNs-Cs in culture media with different pH values of 7.4 and 6.5. As shown in Fig. 6a, the 24 h cell viability decreased

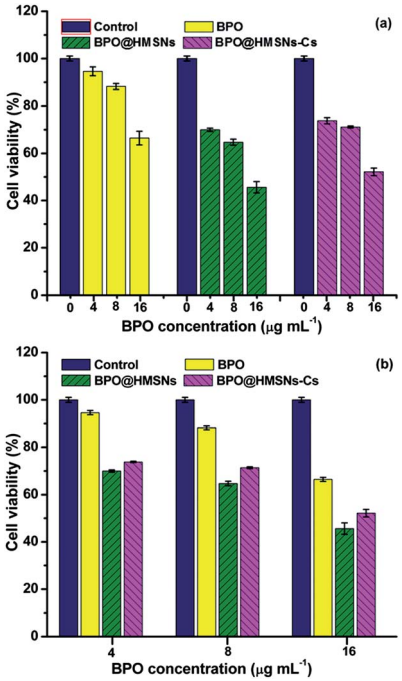

Fig. 5 *In vitro* cytotoxicity of BPO, BPO@HMSNs and BPO@HMSNs-Cs against ZR75-30 cells after 24 h co-incubation in RPMI-1640 media (pH 7.4), supplemented with 10% FBS. (a) Cytotoxicity of the three samples with 4, 8 and 16 μg mL^{-1} of BPO. Culture media without samples were used as negative controls. All samples exhibited incremental cytotoxicity against ZR75-30 cells with increased BPO concentration. (b) Cytotoxicity comparison of the three samples with equivalent BPO concentration (4, 8 and 16 μg mL^{-1}). BPO-loaded nanocomposites exhibited significantly higher cytotoxic effects against ZR75-30 cells compared with free BPO with equivalent BPO concentration. All results were presented as means ± SDs ($n = 6$).

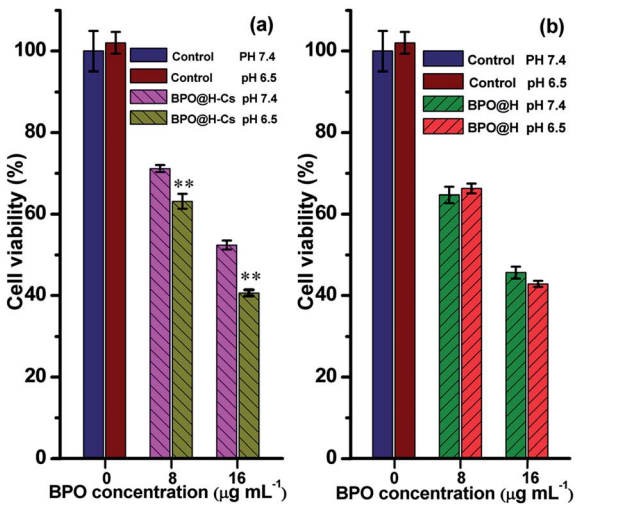

Fig. 6 *In vitro* cytotoxicity of (a) BPO@H-Cs (abbreviation for BPO@HMSNs-Cs) and (b) BPO@H (abbreviation for BPO@HMSNs) against ZR75-30 cells after co-incubation for 24 h in pH 7.4 or 6.5 media. The cytotoxicity of BPO@H-Cs exhibited distinct pH sensitivity. Significantly enhanced cytotoxicity against ZR75-30 cells occurred at acidic pH 6.5 than that at physiological pH 7.4 with equivalent BPO concentration of 8 and 16 μg mL^{-1} (**$P < 0.01$). Comparatively, BPO@H showed no obvious cytotoxicity difference in culture media of pH 7.4 and 6.5 ($P > 0.05$). Data were represented as means ± SDs ($n = 6$).

from 71.1% to 52.2% with 8 μg mL^{-1} of BPO and decreased from 63.2% to 40.6% with 16 μg mL^{-1} of BPO when the media pH changed from 7.4 to 6.5. The cytotoxicity of BPO@HMSNs-Cs exhibited obvious pH dependence and significantly higher cytotoxicity effects occurred at the acidic pH 6.5 than that at the physiological pH 7.4 both at BPO concentrations of 8 and 16 μg mL^{-1} (**$P < 0.01$). For comparison, the cytotoxicity of naked BPO@HMSNs was also evaluated in different pH media. As shown in Fig. 6b, the cytotoxicity of BPO@HMSNs exhibited little pH relevance and no significant toxicity difference in culture media of pH 7.4 and 6.5 ($P > 0.05$). The 24 h cell viability was 64.7%, 66.3% with 8 μg mL^{-1} of BPO and 45.6%, 42.9% with 16 μg mL^{-1} of BPO when the media pH changed from 7.4 to 6.5. Notably, the negative control showed no cytotoxicity effect in both culture media. Furthermore, as shown in Fig. S7,† both nanocarriers (HMSNs and HMSNs-Cs) showed no obvious cytotoxicity difference in culture media of pH 7.4 and 6.5 ($P > 0.05$). It can be concluded that the observed cytotoxicity difference of BPO@HMSNs-Cs was attributed to the increased BPO release at pH 6.5, which further led to the observed higher cytotoxicity. This pH-responsive-enhanced cytotoxicity to diseased tissues of BPO@HMSNs-Cs could alleviate its side effects to normal tissues/organs, which is of great physiological significance.

To further demonstrate that the cytotoxicity of BPO@HMSNs and BPO@HMSNs-Cs were enhanced by the activated BPO, benzoic acid (BA), which is the major stable metabolite of BPO,[38] was also investigated by MTT assay for comparison. As noted in Fig. 7a, 106.4%, 112.9%, 109.8% and 106.3% viability was maintained with BA concentration of 8, 16, 32 and 64 μg mL^{-1} after 24 h exposure. These data indicated that BA showed no obvious cytotoxic effect compared with BPO. Thus, it can be concluded that the observed cytotoxicity in BPO@HMSNs and BPO@HMSNs-Cs was from BPO rather than its stable metabolites. As shown in the molecule structures in Fig. 7b, BA is analogous to BPO except the absence of the peroxide (O–O) bond. The distinct cytotoxicity in BPO and BA was supposed to be from the active O–O bond in the BPO molecule. Previous studies[59] proposed that the metabolism of BPO to BA proceeded *via* a free-radical mechanism; *i.e.*, the O–O bonds in BPO underwent cleavage to yield benzoyloxy radicals. The resulting radicals further fragmented to phenyl radicals or abstract H atoms from biomolecules to form BA. Moreover, it was noted that DNA damage was caused by BPO but not by BA in a cell-free system.[59] These observations collectively support, in part, the hypothesis that the cytotoxic actions of BPO were presumably involved with the generation of free-radical derivations.

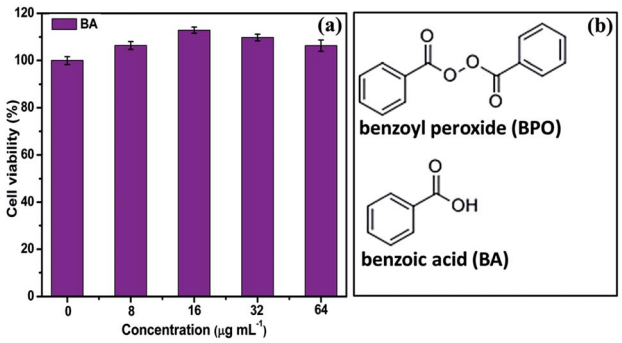

Fig. 7 (a) *In vitro* cytotoxicity of benzoic acid (BA) against ZR75-30 cells after co-incubation for 24 h. (b) Chemical structures of BPO and BA. Compared with BPO, BA showed no obvious cytotoxic effect even at a concentration as high as 64 μg mL^{-1}. The chemical structure of BA is analogous to BPO except that the O–O bond is absent.

Observation of intracellular free-radical production by fluorescence microscopy

2′,7′-Dichlorodihydrofluorescein diacetate (DCFH-DA) is a widely used fluorescence probe to detect free-radical derivations. DCFH-DA itself is non-fluorescent but can penetrate into cells where it is cleaved and oxidized by oxygen free radicals to highly fluorescent 2′,7′-dichlorofluorescein (DCF). To further identify that the cytotoxicity of BPO was involved in free-radical intermediates, DCFH-DA (10 μM in DMSO) was added to the culture media after the cells were exposed to BPO@HMSNs-Cs (140 μg mL^{-1}, containing 16 μg mL^{-1} of BPO) or free BA (16 μg mL^{-1}) for 4 h. After further incubation for 30 min, cells were subjected to fluorescence microscopy observation. Fig. 8 shows the fluorescence images of ZR75-30 cells exposed BPO@HMSNs-Cs and BA. As shown in Fig. 8a, noticeable green fluorescence was observed in the cells exposed to BPO@HMSNs-Cs, indicating the presence of oxygen free radicals during the BPO@HMSNs-Cs metabolism. In contrast, when cells were exposed to equivalent BA, negligible fluorescence could be observed in the cells. As shown in Fig. 7b, the chemical structure of BA is analogous to BPO except that the O–O bond is absent. Previous studies have proposed that the metabolism of BPO to BA proceeded *via* a free-radical mechanism. It can be speculated that the free-radical intermediates generated during BPO@HMSNs-Cs metabolism had promoted the noticeable intracellular green DCF fluorescence.

In order to further ascertain that the noticeable intracellular green DCF fluorescence of BPO@HMSNs-Cs was from the

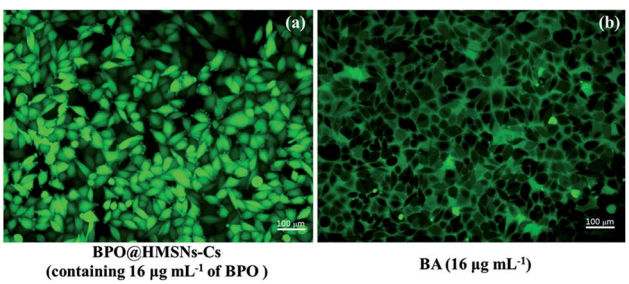

Fig. 8 Fluorescence images of ZR75-30 cells after 4 h exposure to (a) BPO@HMSNs-Cs (140 μg mL^{-1}, containing 16 μg mL^{-1} of BPO) and (b) BA (16 μg mL^{-1}) in serum-free culture media. Noticeable green fluorescence was observed in the cells exposed to BPO@HMSNs-Cs, whereas negligible fluorescence was observed in cells treated with equivalent BA. The free-radical intermediates generated during BPO@HMSNs-Cs metabolism was speculated to promote the noticeable green DCF fluorescence in the cells *via* the reaction with DCFH-DA.

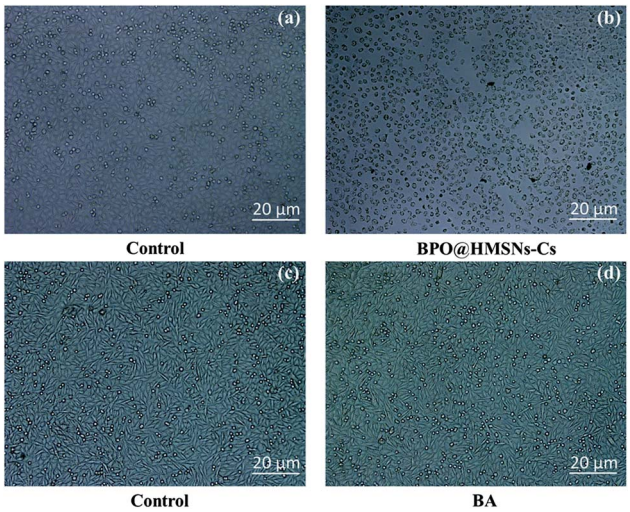

Fig. 9 Microscopic images of ZR75-30 cells exposed to (a and c) fresh culture media without test samples (negative controls), (b) BPO@HMSNs-Cs (140 μg mL^{-1}, containing 16 μg mL^{-1} of BPO) and (d) BA (64 μg mL^{-1}) for 24 h. The cells in control groups were spindly and grew with favorable adherence after 24 h culture. When the cells were exposed to BPO@HMSNs-Cs with 16 μg mL^{-1} of BPO, distinct multi-nucleation and extensive vacuolization were observed. However, small effects were noted on the morphology of cells when exposed to BA even at a concentration as high as 64 μg mL^{-1}.

metabolism of BPO, the cells were also treated with HMSNs-Cs (100 μg mL^{-1}) and observed by fluorescence microscopy after 4 h incubation. As shown in Fig. S8,† negligible intracellular fluorescence was observed in the cells exposed to HMSNs-Cs. It can be concluded that the observed green fluorescence in the cells treated with BPO@HMSNs-Cs (Fig. 8a) was from the oxidizing BPO but not from the HMSNs-Cs carriers.

Observation of cells morphology by inverted microscopy

Microscopic observation was utilized to explore the cells morphology aberration before and after exposure to BPO@HMSNs-Cs and BA. As presented in Fig. 9, cells without test samples (negative controls) were spindly and well maintained with favorable adherence after 24 h (Fig. 9a and c). However, when cells were exposed to BPO@HMSNs-Cs with 16 μg mL^{-1} of BPO, distinct multinucleation and extensive vacuolization were observed, and most cells showed deteriorative adherence (Fig. 9b). Comparatively, small effects were noted on the morphology of the cells when exposed to BA even at a concentration as high as 64 μg mL^{-1} (Fig. 9d). These results were consistent with the cytotoxicity results of BPO@HMSNs-Cs and BA.

Conclusions

To conclude, we develop a controlled, free-radical generation strategy for cancer therapy *via* pH-responsive release of benzoyl peroxide (BPO) as the free-radical resource in acidic tumor media and exerting enhanced toxicologic effects against tumor cells. The poorly soluble BPO was encapsulated into a chitosan (Cs)-coated mesoporous silica nanocomposite (BPO@HMSNs-Cs), which offers many advantages, including enhanced BPO chemical stability, improved BPO aqueous solubility, controlled BPO delivery, as well as more effective BPO uptake, and tumor cell-targeted BPO cytotoxicity. The mesoporous silica carrier improved the solubility and stability of the BPO by preventing its crystallization and stabilizing the amorphous BPO therein. The chitosan imparted the nanocomposite enhanced BPO release in simulated acidic tumor media (pH 6.5) and minor release at simulated normal tissues (pH 7.4). Furthermore, significantly higher BPO@HMSNs-Cs cytotoxicity was realized at tumor acidic pH 6.5 than that at physiological pH 7.4 ($^{**}P < 0.01$). The free radical-mediated toxicological effect of BPO@HMSNs-Cs was demonstrated by the strong green DCF fluorescence in cells, which was induced by the reaction of oxygen free radicals with DCFH-DA. Taken together, this pH-responsive hybrid nanocomposite is potentially applicable for drug-delivery systems in cancer diagnosis and therapy.

Acknowledgements

This work was supported by the National Natural Science Foundation of China (51072217), the Science and Technology Commission of Shanghai Municipality (11XD1405600) and the National High Technology Research and Development Program of China (2008AAO3Z303).

Notes and references

1 W. Droge, *Physiol. Rev.*, 2002, **82**, 47–95.
2 A. P. Breen and J. A. Murphy, *Free Radical Biol. Med.*, 1995, **18**, 1033–1077.
3 R. S. Sohal and R. Weindruch, *Science*, 1996, **273**, 59–63.
4 B. Halliwell and C. E. Cross, *Environ. Health Perspect.*, 1994, **102**, 5–12.
5 P. Venditti, M. Balestrieri, T. De Leo and S. Di Meo, *Cardiovasc. Res.*, 1998, **38**, 695–702.
6 P. Huang, L. Feng, E. A. Oldham, M. J. Keating and W. Plunkett, *Nature*, 2000, **407**, 390–395.
7 S. Gupta, L. Yel, D. Kim, C. Kim, S. Chiplunkar and S. Gollapudi, *Mol. Cancer Ther.*, 2003, **2**, 711–719.
8 J. S. Hong, H. H. Ko, E. S. Han and C. S. Lee, *Biochem. Pharmacol.*, 2003, **66**, 1297–1306.
9 T. J. Slaga, A. J. P. Kleinszanto, L. L. Triplett, L. P. Yotti and J. E. Trosko, *Science*, 1981, **213**, 1023–1025.
10 K. Nozaki and P. D. Bartlett, *J. Am. Chem. Soc.*, 1946, **68**, 1686–1692.
11 Physico-chemical properties of benzoyl peroxide (BPO) obtained from the Syracuse Research Corporation database, http://www.syrres.com/esc/databases.htm.
12 V. B. Patel, A. N. Misra and Y. S. Marfatia, *Drug Dev. Ind. Pharm.*, 2001, **27**, 863–869.
13 M. Jelvehgari, M. R. Siahi-Shadbad, S. Azarmi, G. P. Martin and A. Nokhodchi, *Int. J. Pharm.*, 2006, **308**, 124–132.
14 J. Shim, H. S. Kang, W. S. Park, S. H. Han, J. Kim and I. S. Chang, *J. Controlled Release*, 2004, **97**, 477–484.
15 J. L. Shi, *Chem. Rev.*, 2013, **113**, 2139–2181.

16 J. L. Vivero-Escoto, R. C. Huxford-Phillips and W. B. Lin, *Chem. Soc. Rev.*, 2012, **41**, 2673–2685.
17 X. J. Yang, Z. H. Li, M. Li, J. S. Ren and X. G. Qu, *Chem. –Eur. J.*, 2013, **19**, 15378–15383.
18 Z. H. Li, Y. Tao, S. Huang, N. Gao, J. S. Ren and X. G. Qu, *Chem. Commun.*, 2013, **49**, 7129–7131.
19 Q. J. He and J. L. Shi, *J. Mater. Chem.*, 2011, **21**, 5845–5855.
20 K. T. Mody, A. Popat, D. Mahony, A. S. Cavallaro, C. Z. Yu and N. Mitter, *Nanoscale*, 2013, **5**, 5167–5179.
21 Y. Zhu, J. Shi, W. Shen, X. Dong, J. Feng, M. Ruan and Y. Li, *Angew. Chem., Int. Ed.*, 2005, **117**, 5213–5217.
22 Z. X. Li, J. C. Barnes, A. Bosoy, J. F. Stoddart and J. I. Zink, *Chem. Soc. Rev.*, 2012, **41**, 2590–2605.
23 S. A. Mackowiak, A. Schmidt, V. Weiss, C. Argyo, C. von Schirnding, T. Bein and C. Brauchle, *Nano Lett.*, 2013, **13**, 2576–2583.
24 P. P. Yang, S. L. Gai and J. Lin, *Chem. Soc. Rev.*, 2012, **41**, 3679–3698.
25 J. L. Vivero-Escoto, I. I. Slowing and V. S. Y. Lin, *Biomaterials*, 2010, **31**, 1325–1333.
26 S. H. Wu, C. Y. Mou and H. P. Lin, *Chem. Soc. Rev.*, 2013, **42**, 3862–3875.
27 F. Q. Tang, L. L. Li and D. Chen, *Adv. Mater.*, 2012, **24**, 1504–1534.
28 Q. Gan, X. Y. Lu, W. J. Dong, Y. Yuan, J. C. Qian, Y. S. Li, J. L. Shi and C. S. Liu, *J. Mater. Chem.*, 2012, **22**, 15960–15968.
29 F. Li, Y. C. Zhu, Z. Y. Mao, Y. L. Wang, Q. C. Ruan, J. L. Shi and C. Q. Ning, *J. Mater. Chem. B*, 2013, **1**, 1579–1583.
30 Y. Zhu and M. Fujiwara, *Angew. Chem., Int. Ed.*, 2007, **46**, 2241–2244.
31 Y. C. Zhu, H. J. Liu, F. Li, Q. C. Ruan, H. Wang, M. Fujiwara, L. Z. Wang and G. Q. Lu, *J. Am. Chem. Soc.*, 2010, **132**, 1450.
32 H. Y. Tang, J. Guo, Y. Sun, B. S. Chang, Q. G. Ren and W. L. Yang, *Int. J. Pharm.*, 2011, **421**, 388–396.
33 H. Meng, M. Xue, T. Xia, Z. X. Ji, D. Y. Tarn, J. I. Zink and A. E. Nel, *ACS Nano*, 2011, **5**, 4131–4144.
34 X. L. Fang, C. Chen, Z. H. Liu, P. X. Liu and N. F. Zheng, *Nanoscale*, 2011, **3**, 1632–1639.
35 Y. Chen, Q. Yin, X. F. Ji, S. J. Zhang, H. R. Chen, Y. Y. Zheng, Y. Sun, H. Y. Qu, Z. Wang, Y. P. Li, X. Wang, K. Zhang, L. L. Zhang and J. L. Shi, *Biomaterials*, 2012, **33**, 7126–7137.
36 F. Chen and Y. Zhu, *Microporous Mesoporous Mater.*, 2012, **150**, 83–89.
37 A. Popat, J. Liu, G. Q. Lu and S. Z. Qiao, *J. Mater. Chem.*, 2012, **22**, 11173–11178.
38 S. Nacht, D. Yeung, J. N. Beasley, M. D. Anjo and H. I. Maibach, *J. Am. Acad. Dermatol.*, 1981, **4**, 31–37.
39 E. Marchesi, C. Rota, Y. C. Fann, C. F. Chignell and R. P. Mason, *Free Radical Biol. Med.*, 1999, **26**, 148–161.
40 F. Chen and Y. C. Zhu, *Microporous Mesoporous Mater.*, 2012, **150**, 83–89.
41 J. S. Chang, Z. L. Kong, D. F. Hwang and K. L. B. Chang, *Chem. Mater.*, 2006, **18**, 1714.
42 H. X. Liu, S. Q. Sun, G. H. Lv and K. K. C. Chan, *Spectrochim. Acta, Part A*, 2006, **64**, 321–326.
43 G. Lawrie, I. Keen, B. Drew, A. Chandler-Temple, L. Rintoul, P. Fredericks and L. Grondahl, *Biomacromolecules*, 2007, **8**, 2533–2541.
44 P. Chandra, H. B. Noh and Y. B. Shim, *Chem. Commun.*, 2013, **49**, 1900–1902.
45 V. Ambrogi, F. Marmottini and C. Pagano, *Microporous Mesoporous Mater.*, 2013, **177**, 1–7.
46 T. Limnell, T. Heikkila, H. A. Santos, S. Sistonen, S. Hellsten, T. Laaksonen, L. Peltonen, N. Kumar, D. Y. Murzin, M. Louhi-Kultanen, J. Salonen, J. Hirvonen and V. P. Lehto, *Int. J. Pharm.*, 2011, **416**, 242–251.
47 M. F. Bennewitz, T. L. Lobo, M. K. Nkansah, G. Ulas, G. W. Brudvig and E. M. Shapiro, *ACS Nano*, 2011, **5**, 3438–3446.
48 M. Sax and R. K. Mcmullan, *Acta Crystallogr.*, 1967, **22**, 281–288.
49 M. Yalpani and L. D. Hall, *Macromolecules*, 1984, **17**, 272–281.
50 K. Okuyama, K. Noguchi, T. Miyazawa, T. Yui and K. Ogawa, *Macromolecules*, 1997, **30**, 5849–5855.
51 M. N. V. R. Kumar, R. A. A. Muzzarelli, C. Muzzarelli, H. Sashiwa and A. J. Domb, *Chem. Rev.*, 2004, **104**, 6017–6084.
52 P. M. Biesheuvel, T. Mauser, G. B. Sukhorukov and H. Mohwald, *Macromolecules*, 2006, **39**, 8480–8486.
53 Y. Chen, H. R. Chen, D. P. Zeng, Y. B. Tian, F. Chen, J. W. Feng and J. L. Shi, *ACS Nano*, 2010, **4**, 6001–6013.
54 I. I. Slowing, J. L. Vivero-Escoto, C. W. Wu and V. S. Y. Lin, *Adv. Drug Delivery Rev.*, 2008, **60**, 1278–1288.
55 S. D. Conner and S. L. Schmid, *Nature*, 2003, **422**, 37–44.
56 S. Mornet, O. Lambert, E. Duguet and A. Brisson, *Nano Lett.*, 2005, **5**, 281–285.
57 J. Lu, M. Liong, J. I. Zink and F. Tamanoi, *Small*, 2007, **3**, 1341–1346.
58 X. L. Huang, X. Teng, D. Chen, F. Q. Tang and J. Q. He, *Biomaterials*, 2010, **31**, 438–448.
59 J. E. Swauger, P. M. Dolan, J. L. Zweier, P. Kuppusamy and T. W. Kensler, *Chem. Res. Toxicol.*, 1991, **4**, 223–228.

